analytical chemistry

Article

Cite This: *Anal. Chem.* 2019, 91, 6569−6576

pubs.acs.org/ac

Highly Stretchable and Strain-Insensitive Fiber-Based Wearable Electrochemical Biosensor to Monitor Glucose in the Sweat

Yunmeng Zhao,[†,‡] Qingfeng Zhai,[†,‡] Dashen Dong,[†,‡] Tiance An,[†,‡] Shu Gong,[†,‡] Qianqian Shi,[†,‡] and Wenlong Cheng*[,†,‡]

[†]Department of Chemical Engineering, Monash University, Clayton, Victoria 3800, Australia

[‡]The Melbourne Centre for Nanofabrication, Clayton, Victoria 3800, Australia

Supporting Information

ABSTRACT: Development of high-performance fiber-shaped wearable sensors is of great significance for next-generation smart textiles for real-time and out-of-clinic health monitoring. The previous focus has been mainly on monitoring physical parameters such as pressure and strains associated with human activities. Development of an enzyme-based non-invasive wearable electrochemical sensor to monitor biochemical vital signs of health such as the glucose level in sweat has attracted increasing attention recently, due to the unmet clinical needs for the diabetic patients. To achieve this, the key challenge lies in the design of a highly stretchable fiber with high conductivity, facile enzyme immobilization, and strain-insensitive properties. Herein, we demonstrate an elastic gold fiber-based three-electrode electrochemical platform that can meet the aforementioned criteria toward wearable textile glucose biosensing. The gold fiber could be functionalized with Prussian blue and glucose oxidase to obtain the working electrode and modified by Ag/AgCl to serve as the reference electrode; and the nonmodified gold fiber could serve as the counter electrode. The as-fabricated textile glucose biosensors achieved a linear range of 0−500 μM and a sensitivity of 11.7 μA mM^{-1} cm^{-2}. Importantly, such sensing performance could be maintained even under a large strain of 200%, indicating the potential applications in real-world wearable biochemical diagnostics from human sweat.

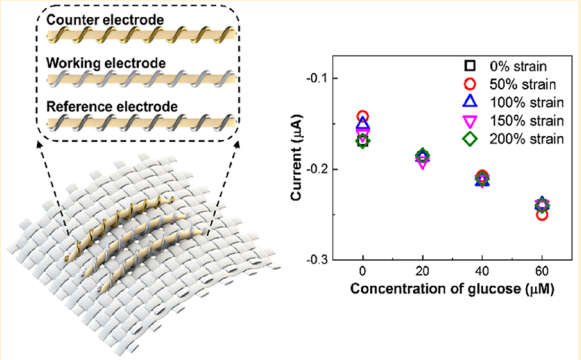

Wearable sensors have attracted increasing attention due to their potential applications in continuous, real-time, and out-of-clinic health monitoring.[1−9] Among various health-related physical and chemical sensors that have been intensely investigated in the past decade, the glucose sensor is of high significance, for diabetes is one of the most common chronic diseases, which leads to catastrophic results nationally and globally.[10,11] Due to the uncontrollable blood glucose level caused by diabetes, patients have to take daily medication based on the guidance of the frequent blood glucose checks. To relieve patients from physical pain and psychological stress induced by the traditional blood sampling from the fingertip, the non-invasive and wearable glucose sensors to monitor sweat glucose, which is related to blood glucose,[12,13] are highly desirable. Since human sweat has complex chemical mixtures, it is crucial to realize high selectivity, and the enzymatic glucose biosensor is the prime candidate due to the high selectivity and sensitivity offered by glucose oxidase.[14−16]

It is encouraging to see some impressive flexible non-invasive enzyme-based glucose sensors reported recently in the literature.[17−20] Ideally, such flexible sensors may function under stretched states since human skin is highly elastic.[21,22] Nevertheless, it is nontrivial to design highly stretchable glucose biosensors since conductivity and the active surface of electrodes tend to change by strain.[22,23] The stretchability of wearable biosensors may be realized either by the use of intrinsically stretchable electrodes or the extrinsically stretchable structures.[24,25] Extrinsic structural design by the use of serpentine shapes dominates in the reported electrochemical biosensors.[26,27] Due to the dynamic nature of the soft, wrinkled, and irregular skin, it is usually challenging to establish conformal contact between patches and human skin, especially under severe deformations. In addition, these elastomeric patches are usually waterproof, possibly resulting in an uncomfortable and unbreathable wearing experience.[28]

The past several years have witnessed the growing interest in fiber-based wearable electronics, which can be produced by spinning technique in a scalable manner and lead to textile wearables that can have excellent wearing experiences.[29−31] With the aid of the efficient knitting and weaving technologies, functional fibers can be integrated into multifunctional textiles, and the order structure of textile is naturally suitable for an electrochemical sensor composed of three adjacent electrodes. Besides, the knitting/weaving structures can provide external stretchability to the device.[32] However, to our best knowledge, a stretchable enzyme-based fiber or textile glucose sensor is not

Received: January 10, 2019
Accepted: April 22, 2019
Published: April 22, 2019

DOI: 10.1021/acs.analchem.9b00152
Anal. Chem. 2019, 91, 6569−6576

yet reported, which may be due to the challenge of preparing highly stretchable, conductive, and strain-insensitive fiber electrodes.

Due to high chemical inertness, excellent biocompatibility, and large surface area, gold nanomaterials have shown qualification as a high-performance material in electrochemical devices.[33] For instance, gold nanoparticles (AuNPs) and gold nanowires (AuNWs) have been reported to build high-performance stretchable electrochemical supercapacitors.[34−36] And, recently, gold nanomaterials-based electrodes were reported to have the capability in various stretchable biological analyses, indicating great promise in wearable electrochemical biosensors.[37−40]

Herein, we demonstrated the preparation and application of an all-gold-fiber-based stretchable three-electrode electrochemical biosensing platform for enzyme-based wearable glucose detection. Built upon our earlier success in producing the stretchable gold fibers by dry spinning and electroless plating,[41,42] we further coated the fibers with a thin layer of Ag/AgCl or Prussian blue (PB) by electrodeposition by cyclic voltammetry methods. Our studies show such coating did not alter much the intrinsic stretchability of functionalized fibers. The Au/AgCl-modified fiber could serve as the reference electrode and PB-modified fibers were further modified with glucose oxidase (GOx) to serve as the working electrode, whereas nonmodified gold fibers were used as counter electrodes. Further winding such functional fibers around elastic fiber cores enabled excellent electrochemical performances under 200% strains. We could achieve a sensitivity of 11.7 μA mM^{-1} cm^{-2} toward glucose detection under a highly stretched state and a high selectivity to be able to monitor the glucose level in artificial sweat. The results demonstrated here indicate the potential application in wearable textile-based biodiagnostics.

EXPERIMENT SECTION

Materials. The chemicals used were as follows: $HAuCl_4 \cdot 3H_2O$ (Sigma-Aldrich), oleylamine (OA; Sigma-Aldrich), triisopropylsilane (TIPS; Sigma-Aldrich), *n*-hexane (Merck), styrene−ethylene/butylene−styrene (SEBS) (G1651H, Kraton), silicone oil (Sigma-Aldrich), tetrahydrofuran (THF; Thermo Fisher Scientific), acetone (Thermo Fisher Scientific), ethanol (Thermo Fisher Scientific), 4-mercaptobenzoic acid (MBA; Sigma-Aldrich), L-ascorbic acid (L-AA; Sigma-Aldrich), $NaBH_4$ (Sigma-Aldrich), sulfuric acid (H_2SO_4; J.T Baker), $K_3Fe(CN)_6$ (Sigma-Aldrich), KCl (Sigma-Aldrich), NaCl (Sigma-Aldrich), $FeCl_3$ (Sigma-Aldrich), glucose (Sigma-Aldrich), glucose oxidase (GOx) from *Aspergillus niger* (Sigma-Aldrich), bovine serum albumin (BSA; Sigma-Aldrich), urea (Sigma-Aldrich), lactic sodium (Sigma-Aldrich), uric acid (Sigma-Aldrich), NaH_2PO_4 (Sigma-Aldrich), Na_2HPO_4 (Sigma-Aldrich), chitosan (Sigma-Aldrich), KNO_3 (Sigma-Aldrich), and $AgNO_3$ (Sigma-Aldrich). The elastic fiber core is a commercially available double covered yarn made of a latex rubber core covered with nylon fibers. And before using, the elastic fiber core was sequentially cleaned by 1h sonication in acetone, ethanol, and water. A 0.1 M amount of phosphate-buffered solution (PBS) containing 137 mM NaCl was used (pH 7.4). Artificial sweat composed of 22 mM urea, 5.5 mM lactic acid, 25 μM uric acid, 10 mM KCl, and 137 mM NaCl was prepared according to a literature procedure (pH 5.5).[8] Milli-Q water was used in all experiments (resistivity, 18.2 MΩ cm).

Synthesis of AuNWs. AuNWs were synthesized on the basis of a reported method.[43,44] An 88 mg amount of $HAuCl_4 \cdot 3H_2O$ and 3 mL of OA were added and dissolved in 40 mL of *n*-hexane. Then 4.2 mL of TIPS was added to form an orange stock solution. The stock solution was kept at ambient temperature and in the dark for 2 days until the color of the solution became dark red, indicating the successful synthesis of AuNWs. The synthesis of AuNWs could be scaled up with the same ratio of chemicals. To obtain a high-concentration dispersion of AuNWs and remove excessive OA, 9 mL of ethanol was added to 3 mL of stock solution and the mixed solution was centrifuged at 6000 rpm for 5 min to precipitate AuNWs. The AuNWs were then re-dispersed in THF for the desired concentrations.

Dry Spinning of the AuNWs/SEBS Fiber. A 20 mg amount of AuNWs, 20 mg of silicone oil, and 200 mg of SEBS granules were added into 2 mL of THF, and a well-mixed spinning solution was obtained after being shaken at 1800 rpm for 2 days. The spinning solution was transferred into a 3 mL syringe with a gauge 25 needle. The syringe was set vertically with the needle downward on a syringe pump, and the plunger of the syringe was pushed by the syringe pump at a fixed rate of 4 mL h^{-1}. A stream of spinning solution was extruded into the air and dried rapidly to form a long AuNWs/SEBS fiber, which was then collected with a polyimide plate beneath the needle.

Electroless Plating of the AuFilm. To plate AuFilm on the surface of the AuNWs/SEBS fiber, a AuNWs/SEBS fiber was prestretched to 300% and immersed into an electroless plating solution containing 2.4 mL of absolute ethanol, 0.1 mL of 60 mM MBA solution, 2.64 mL of 25 mM $HAuCl_4 \cdot 3H_2O$ aqueous solution, and 0.4 mL of 400 mM L-AA aqueous solution. After 10 min, the prestretched AuNWs/SEBS was cleaned with water and then immersed in 25 μM $NaBH_4$ aqueous solution for 10 min to remove absorbed MBA. Finally, the fiber was washed with water and released to its original length to form a stretchable Au fiber with wrinkled AuFilms.

Preparation of the Au/Ag/AgCl Reference Electrode. The above-obtained stretchable Au fiber was modified with Ag/AgCl to work as a reference electrode in the biochemical sensor.[21,32] A stretchable Au fiber was immersed in 5 mM $AgNO_3$/1 M KNO_3 solution as an electrolyte. A layer of Ag was electrochemically deposited onto the stretchable Au fiber electrode by cyclic voltammetry from −0.9 to 0.9 V versus a commercial Ag/AgCl electrode at 0.1 V s^{-1} for 14 cycles (a Pt wire was used as the counter electrode). For chlorination, the fiber electrode was immersed in 10 mM KCl/0.1 M HCl solution, and four cycles of cyclic voltammetry from −0.15 to 1.05 V versus a commercial Ag/AgCl electrode at 50 mV s^{-1} were applied (a Pt wire was used as the counter electrode).

Preparation of the Glucose Sensing Electrode. The glucose sensing electrode was prepared by depositing PB and immobilizing GOx onto the stretchable Au fiber.[8] First, an aqueous solution of 2.5 mM $FeCl_3$, 2.5 mM $K_3Fe(CN)_6$, 0.1 M KCl, and 0.1 M HCl was prepared, and a stretchable Au fiber was immersed in the solution. Then the PB mediator layer was electrochemically deposited onto the stretchable Au fiber by cyclic voltammetry from 0 to 0.5 V versus a commercial Ag/AgCl electrode for three cycles to form a Au/PB fiber (a Pt wire was used as the counter electrode). Second, an aqueous solution of 40 mg/mL GOx and 10 mg/mL BSA in 0.1 M PBS buffer, and an aqueous solution of 1 wt % chitosan in 2 wt % acetic acid was prepared. Then 3 μL of GOx/BSA solution was carefully drop-casted onto the Au/PB fiber. Finally, after

DOI: 10.1021/acs.analchem.9b00152
Anal. Chem. 2019, 91, 6569−6576

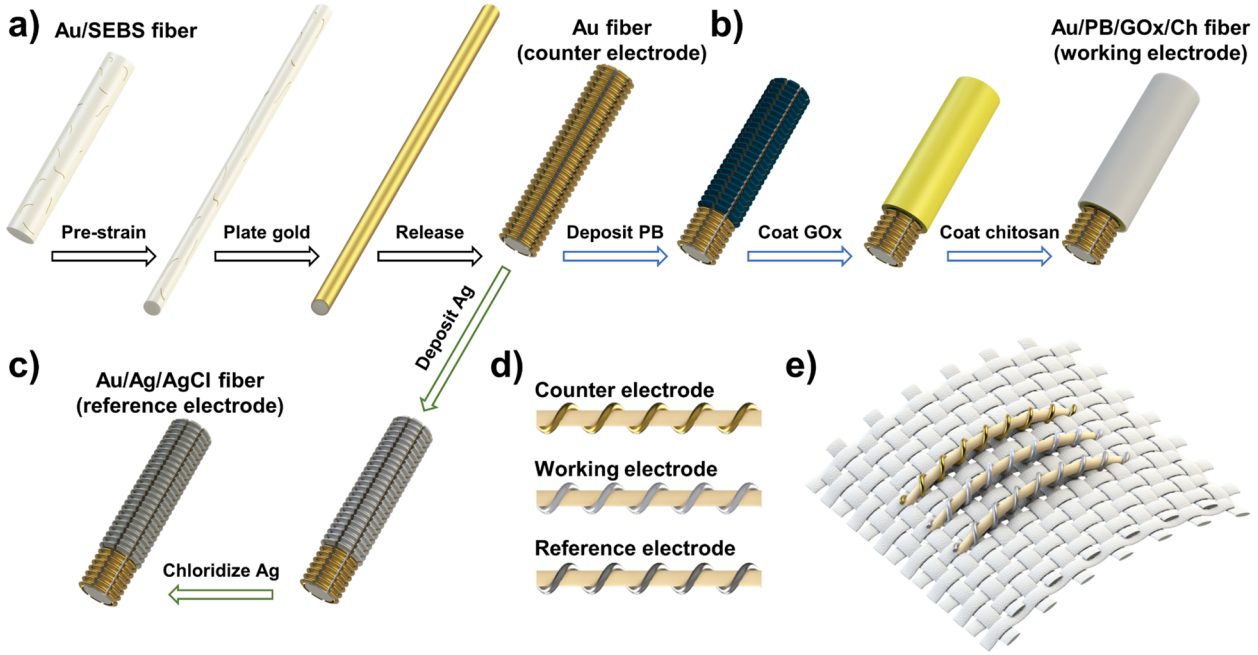

Figure 1. Schematic illustration of the fabrication process of the stretchable fiber-based glucose sensor: (a–c) Schematic illustrations of the fabrication processes of the stretchable Au fiber (counter electrode), the Au/PB/GOx/Ch fiber (working electrode), and the Au/Ag/AgCl fiber (reference electrode), respectively; (d) schematic illustration of the three-electrode glucose sensor; (e) schematic illustration of the glucose sensors integrated into an elastic textile.

drying the fiber electrode under ambient conditions, 12 μL of chitosan solution was drop-casted onto the fiber electrode to form a Au/PB/GOx/Ch fiber electrode.

Assembly of the Glucose Sensor. A nonmodified Au fiber, a Au/Ag/AgCl fiber, and a Au/PB/GOx/Ch fiber worked as a counter electrode, a reference electrode, and a working electrode, respectively. Each fiber electrode was wound helically onto an individual elastic fiber core with the assistance of two rotational motors, and the winding angle was measured by a protractor. One copper wire was connected to each fiber electrode. After winding, three helix fiber electrodes were patterned parallel for sensing glucose.

Characterization. Morphology characterizations were carried out on an FEI Helios Nanolab 600 FIB-SEM at 5 kV and 86 pA, and a Philips CM 20 TEM at 200 kV. Electrical signals were collected by an electrochemical system (VersaSTAT 3, Princeton Applied Research). The sensing performance of the glucose sensor was characterized in 0.1 M PBS buffer solution or artificial sweat in chronoamperometry for 60 s at −0.15 V versus Au/Ag/AgCl fiber electrode at different strains. The selectivity of the glucose sensor was tested in the presence of interfering solutes, namely, 50 μM uric acid, 10 μM ascorbic acid, and 5 mM sodium lactate. The operational stability of the biosensor was continuously tested at a fixed glucose concentration of 100 μM for 6 h. The storage stability of the biosensor was tested at the same glucose concentration of 100 μM for 8 days. After each use, the sensor was washed with water and stored at 4 °C. Yunmeng Zhao (healthy male, 28-year-old), the only volunteer for the on-body sweat glucose test, has given the full consent for the demonstration of the fiber-based wearable electrochemical biosensor and releasing results to the public. The fiber-based glucose sensor was attached to a textile forearm band. Before the test, the volunteer did indoor exercise for 20 min to generate sweat. The chronoamperometric response of the on-body sweat glucose test was recorded at −0.15 V for 60 s at three status, premeal, postmeal 1 h, and postmeal 2 h.

RESULTS AND DISCUSSION

Fabrication of the Fiber Electrodes and the Glucose Sensor. In the first step of fabrication, ultrathin AuNWs were synthesized based on a modified method.[43,44] The ultrathin AuNWs have a diameter of only 2 nm and a large aspect ratio over 1000 (shown in Supporting Information Figure S1). As reported previously, the AuNWs have great dispersibility and compatibility with low polar solvents and polymers.[45,46] Then by using a recently reported dry spinning method (shown in Figure S2), the highly elastic coblock polymer poly(styrene-ethylene–butadiene-styrene) (SEBS) fibers containing 8.33 wt % AuNWs could be produced at a large scale.[41] In brief, AuNWs and SEBS were mixed well in tetrahydrofuran (THF) and then extruded out of a gauge 25 needle into the air vertically. Due to the low boiling point of THF, the extruded stream of solution dried into elastic AuNWs/SEBS fiber in the air.

Figure 1a schematically illustrates the fabrication process of the stretchable Au fiber based on the AuNWs/SEBS fiber. The as-spun AuNWs/SEBS fiber was characterized by scanning electron microscope (SEM) and energy-dispersive X-ray spectroscopy (EDX) mapping (Figure S3). Confirmed with EDX, the Au element from AuNWs were exposed on the surface of the fiber, providing seeds for the electroless gold deposition with strong adhesion. The as-spun AuNWs/SEBS fiber was then prestrained to 300% and immersed into an electroless plating solution of gold, which contained a gold precursor, a complexing agent, and a reducing agent, for 10 min. During the immersion, the AuNWs exposed on the surface of the AuNWs/SEBS fiber provided the initial nucleation areas for the electroless plating process, leading to a dense layer of gold deposited onto the surface of the fiber.[41]

DOI: 10.1021/acs.analchem.9b00152
Anal. Chem. 2019, 91, 6569–6576

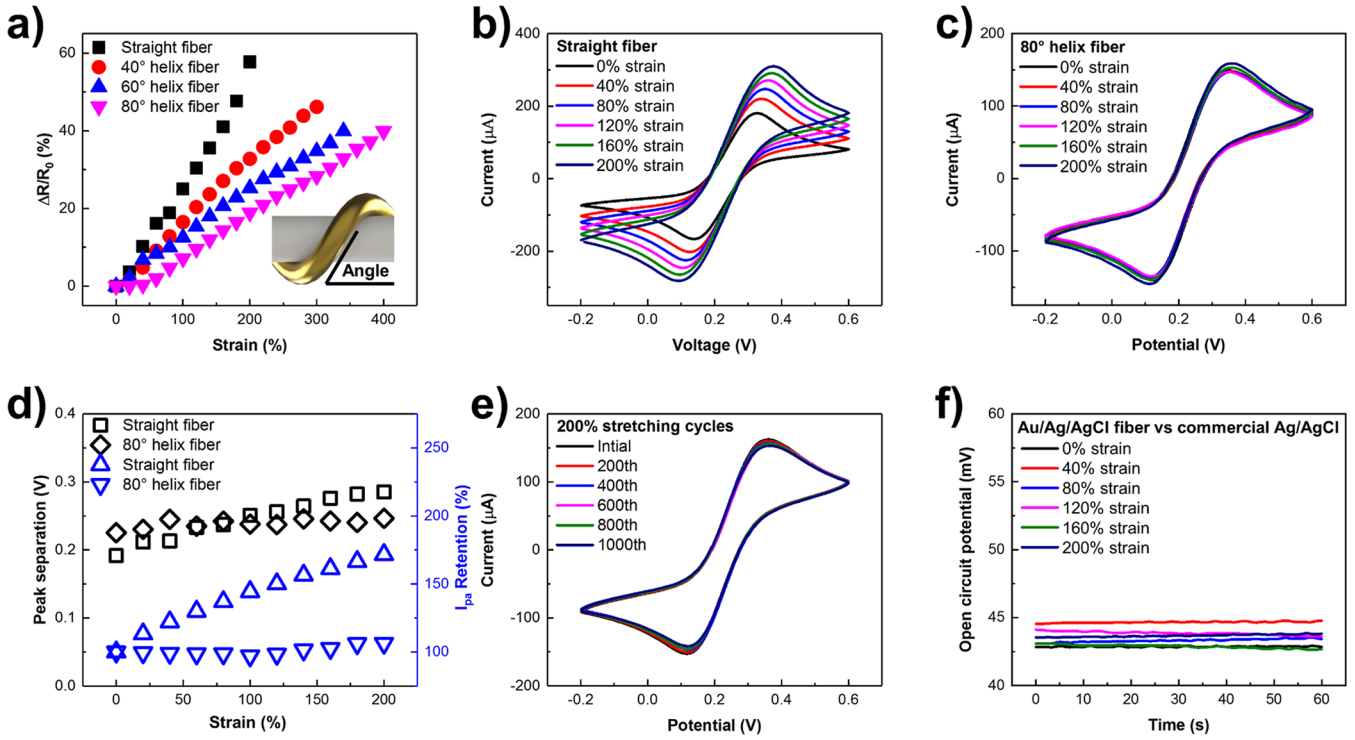

Figure 2. Electrical performance of the stretchable fiber electrodes: (a) Normalized resistance−strain curves of the straight Au fiber and the helix Au fiber with 40, 60, and 80° winding angles, respectively; (b) electrochemical performance of the straight Au fiber from 0 to 200% strain in 5 mM $Fe(CN)_6^{3-/4-}$; (c) electrochemical performance of the 80° helix Au fiber electrode from 0 to 200% strain in 5 mM $Fe(CN)_6^{3-/4-}$; (d) comparison of the electrochemical performance of straight and the 80° helix Au fiber in redox peak separation and reduction peak retention; (e) CV curves during 1000 cycles of 200% stretching/releasing on the 80° helix fiber; (f) open circuit potential of the Au/Ag/AgCl reference fiber versus a commercial Ag/AgCl reference electrode in 0.1 M PBS buffer solution.

After the plating, the fiber was washed with water and immersed into a wet nanowelding solution containing $NaBH_4$. The wet nanowelding process cleaned the surface of the deposited gold and led to the fusion of deposited gold particles into a strong and ductile AuFilm.[47] After being released to the original length, the fused AuFilm wrinkled and cracked due to the dimension change, but still attached firmly to the fiber due to the strong adhesion between gold and elastomer due to the Moss-like AuNWs rooted gold structure, forming the final stretchable Au fiber electrode with wrinkled AuFilm.[41]

The average conductivity of the stretchable Au fibers was about 93 S cm^{-1}, and the stretchable Au fibers could be used as electrochemical fiber electrodes due to their chemical inertness and the high conductivity. The as-prepared stretchable Au fiber could directly work as the counter electrode as well as working and reference electrodes after chemical modifications. For the working electrode, at first, PB was electrodeposited onto the stretchable Au fiber for a Au/PB fiber to facilitate electron transport between redox enzymes and the gold surface (Figure 1b). Glucose enzyme was then drop-casted onto the Au/PB fiber followed by a permeable film of chitosan (Ch), forming a final Au/PB/GOx/Ch fiber as the working electrode. The Au/Ag/AgCl fiber reference electrode was built by electrodepositing a layer of Ag onto the Au fiber, and then the Ag was chloridized into AgCl in an electrochemical cell (Figure 1c).

It is known that the stretchability of a device can be achieved by the use of intrinsically stretchable active materials or extrinsically by virtue of stretchable structure.[25] The wrinkled AuFilms on each electrode were stretchable, and to enhance further the overall stretchability of the glucose sensor, the three electrodes were wound helically around elastic fiber cores (Figure 1d). By assembling three helical fiber electrodes together, the stretchable fiber-based glucose sensor was obtained. The three-electrode electrochemical glucose sensing fibers could be woven into commercially available textiles in a facile manner. We demonstrated this simply by weaving the functional fibers into an everyday elastic sock (Figure S4).

Characterization of the Fiber Electrodes. The wrinkled and cracked AuFilm was characterized by SEM and shown in Figure S5a. The wrinkled surface of AuFilm provided a large surface area to enhance the electrochemical performance. And the electrochemically active surface area (EASA) and the roughness factor (RF) were characterized to investigate the electrochemical performance of the stretchable Au Fiber. To remove the potential surface contaminants, the Au fiber was scanned in 1 M H_2SO_4 at a fixed scan rate of 0.1 V s^{-1} for 20 cycles until stable cyclic voltammetry (CV) curves were generated. The CV curves of the stretchable Au fiber are shown in Figure S6, which is a typical CV curve of gold with the oxidation peak of gold at about 1.3 V and reduction peak of gold oxide at about 0.9 V. EASA and RF were calculated based on the integration of the charge of reducing gold oxide, according eqs 1−3:[48,49]

$$\mathrm{EASA} = Q/c \tag{1}$$

$$Q = A/v \tag{2}$$

$$\mathrm{RF} = A/S \tag{3}$$

where Q is the required charge for reducing gold oxide in the negative sweep, c is the required charge for reducing a

DOI: 10.1021/acs.analchem.9b00152
Anal. Chem. 2019, 91, 6569−6576

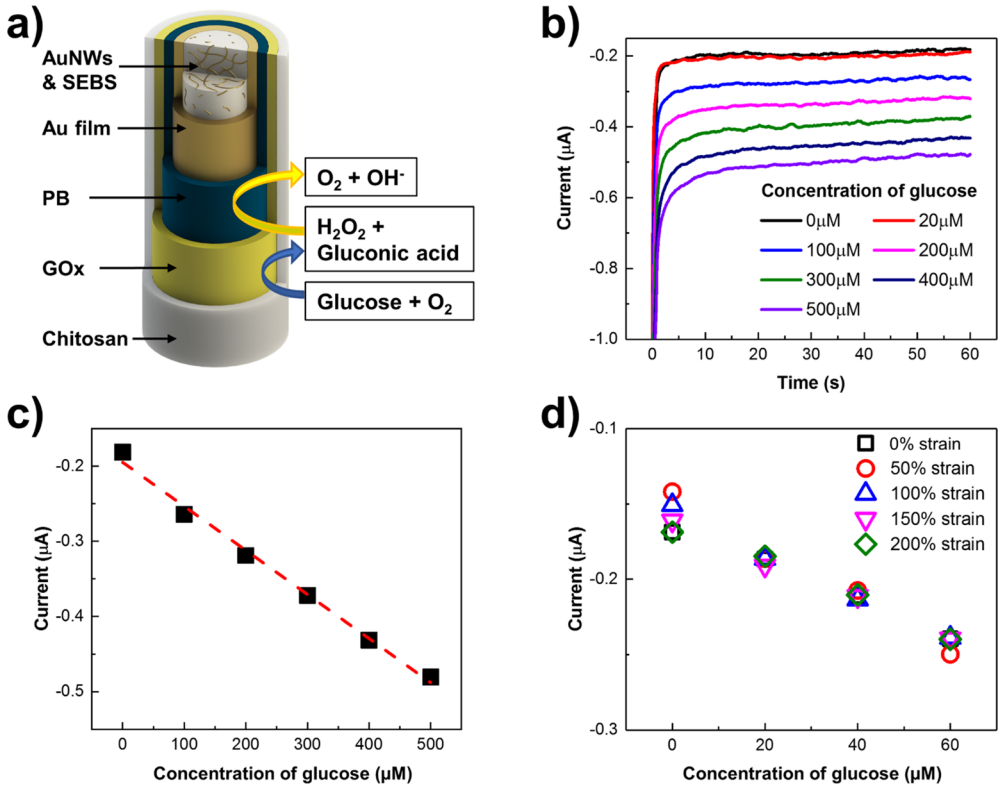

Figure 3. Glucose sensing performance of the stretchable fiber-based glucose sensor in PBS buffer: (a) schematic illustration of the fiber working electrode and the two main reactions on the interface of the electrode and the solution; (b) chronoamperometric responses of the stretchable fiber-based glucose sensor to the increasing glucose concentrations from 0 to 500 μM; (c) corresponding calibration plot of panel b; (d) calibration plot of the chronoamperometric responses of the stretchable fiber-based glucose sensor from 0 to 200% strain.

monolayer of Au oxide (386 μC cm $^{-2}$), A is the integration of the reduction peak of gold oxide, v is the scan rate of the CV sweep, and S is the geometric surface area of the fiber electrode. The EASA of the Au fiber was 0.552 cm^2 with an RF of 11.0, exhibiting large active area.

As shown in Figure S5b,c, the Au/Ag/AgCl fiber and Au/PB fiber had similar wrinkled surfaces with the Au fiber. Figure S7 shows that the chemical map of the Fe element matched well with the surface morphology of the Au/PB fiber, demonstrating the presence of GOx. In the Raman spectrum, three characteristic peaks of Prussian blue were evident, demonstrating the successful modification of Prussian blue. Shown in Figure S5d, the coated GOx and Ch formed a uniform thin layer on the wrinkled surface. These wrinkled surfaces with uniform deposition or coating indicated the intrinsically stretchable nature of the fiber electrodes.

In situ SEM images of the Au fiber, Au/Ag/AgCl fiber, and Au/PB fiber from 0 to 200% strain are shown in Figure S8a−c, respectively. It is notable that all three fiber electrodes showed similar morphology change under strain. With increasing strain, the wrinkled films flattened, and the cracked films were getting closer to each other. And at 200% strain, the wrinkled films became almost flat and the cracks nearly disappeared, leading to a great retention of the conductive pathways. The unique morphology changes of wrinkle flattening and crack disappearing enabled the fiber electrodes with high intrinsic stretchability, which was ideal for electrochemical sensing.

The helical structure is a highly effective strain buffering structure, which has been widely used in various traditional metallic springs and advanced wearable electronics.[50] To optimize the stretchability of the helical structure, the electrical performance of the fiber electrode with different winding angles were carefully investigated in the stretching test. Figure 2a shows that although the straight fiber electrode had a good stretchability of 200% with only 58% increase of resistance, compared to these helical fiber electrodes, the straight fiber electrode still had the smallest stretchability. As expected, with the larger winding angle, the fiber electrode was more stretchable. And the 80° helix fiber exhibited a stretchability of 400% with only a 40% increase in resistance, indicating a great potential to be used as a stretchable electrochemical sensing platform.

To evaluate the electrochemical performance of the fiber electrode, a redox couple, $Fe(CN)_6^{3-/4-}$ was used. As shown in Figure 2b,c, the CV curves of the straight fiber electrode and the 80° helix fiber electrode were recorded from 0 to 200% strain in 5 mM $Fe(CN)_6^{3-/4-}$. Each CV curve showed a typical couple of redox peaks; however, the straight fiber and the 80° helix showed different behaviors under strains. To more clearly and visually present the difference between the electrochemical performances of the two fiber electrodes, two key parameters, the redox peak separation and the reduction peak retention, during stretching cycles were recorded as shown in Figure 2d. The redox peak separation of the straight fiber increased from 0.19 to 0.29 V during 0 to 200% strain, which can be attributed to the increase of resistance under strain. In this process, the reduction peak current increased by about 71% at 200% strain compared to 0% strain due to the increase of surface area during straining. Thus, though the straight fiber electrode showed the capability of working in the strain range of 200%, the increase in the peak separation and the reduction peak current made it less ideal as a stretchable sensing electrode. In

DOI: 10.1021/acs.analchem.9b00152
Anal. Chem. 2019, 91, 6569−6576

comparison, in the strain range of 200%, the CV curves of the 80° helix fiber overlapped, showing almost identical redox peak separations and negligible fluctuation of reduction peak currents. Furthermore, as shown in Figure S9, the 80° helix fiber could be stretched up to 400% without significant change in CV curves. The durability of the helix fiber electrode was tested by 1000 continuous stretching/releasing cycles. As shown in Figure 2e, the CV curves exhibited negligible changes, indicating great reliability and durability. The strain-insensitive electrochemical performance made the 80° helix fiber electrode a promising candidate for stretchable electrochemical sensing. Therefore, the 80° helix fibers were used as the platform for the three-electrode glucose sensor.

The performance of the Au/Ag/AgCl fiber reference electrode was tested in an open circuit potential test versus a commercial bulky Ag/AgCl reference electrode in a 0.1 M PBS. At 0% strain, the Au/Ag/AgCl fiber electrode showed a stable open circuit potential around 43 mV (Figure 2f). This open potential could be well-maintained even under the 200% strain, leading to a highly stretchable and reliable reference for the glucose sensor.

Characterization of the Stretchable Fiber-Based Glucose Sensor. Figure 3a illustrates the structure of the working electrode of the glucose sensor. Two main reactions occur at the interface between the electrode and solution. In the first reaction, glucose is oxidized with the assistance of the GOx, and two products, gluconic acid and H_2O_2, are generated. PB could facilitate the electron transfer between GOx and the gold surface, enabling low-potential detection of H_2O_2. The low-potential detection is critical for electrochemical sensing in the sweat because the high potential may cause signal interferences.[16] The chronoamperometry at −0.15 V was deployed to investigate the sensitivity toward glucose of the stretchable fiber-based glucose sensor. As shown in Figure 3b, the glucose sensor was demonstrated with clear and quantitative response to the increasing concentrations of glucose. Shown in Figure 3c, the calibration plotting and fitting exhibit a linear response toward glucose in the range of glucose level in the sweat (from 0 to 500 μM, R^2 = 0.992). And a sensitivity of 11.7 μA mM^{-1} cm^{-2} was achieved. A limit of detection (LOD) of 6 μM was calculated referring to eq 4:[51]

$$\mathrm{LOD} = 3S_b/S \tag{4}$$

where S_b is the standard deviation of the blank signal and S is the sensitivity.

We further evaluated the glucose sensing performance under stretched states, which is critical for real-world on-body applications where sensors may be deformed for routine human activities. This was investigated by chronoamperometry. The calibration plots of the glucose sensor from 0 to 200% strain are shown in Figure 3d. Notably, within 200% strain, the sensor recorded comparable currents for respective glucose concentrations.

The performance of our glucose sensor was compared with those of previous flexible and stretchable glucose sensors (Table S1). Among various parameters, we note that the workable strain range of our sensor was much wider than those of the previously reported fiber-based glucose sensor.[52]

We further assessed the selectivity of the glucose sensor in the artificial sweat using the chronoamperometry. In the artificial sweat, some interfering molecules including uric acid, ascorbic acid, and sodium lactate were added to concentrations which are comparable to those in the human sweat. The corresponding chronoamperometric responses were collected. Finally, the stock solution of glucose was added, and the response of the sensor was also collected. Figure 4a shows that

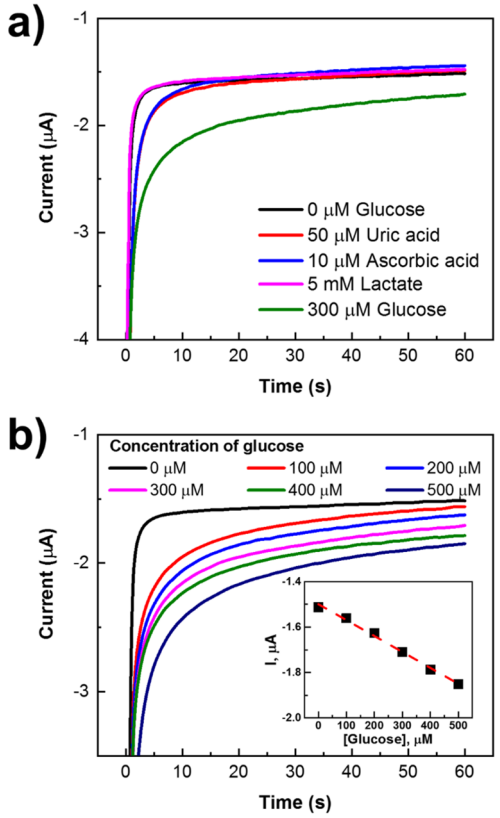

Figure 4. Glucose sensing performance of the stretchable fiber-based glucose sensor in artificial sweat: (a) interference study by subsequent additions of 50 μM uric acid, 10 μM ascorbic acid, 5 mM sodium lactate, and 300 μM glucose; (b) chronoamperometric responses of the stretchable fiber-based glucose sensor to the increasing glucose concentrations from 0 to 500 μM. The inset shows the corresponding calibration plot. Medium, artificial sweat.

although the interfering species caused some minor fluctuation in the electrochemical responses, the glucose sensor showed sharp response toward the addition of glucose, attributed to the selective oxidation of the immobilized GOx and relatively low potential with the assistance of PB.[19,21] In addition, the sensitivity of the glucose sensor in artificial sweat was demonstrated by altering glucose concentration (Figure 4b). For the concentration range of 0−500 μM, we could achieve a sensitivity of 13.9 μA mM^{-1} cm^{-2} by a linear fit (R^2 = 0.993). This was comparable to the sensitivity achieved in the PBS buffer solution.

Besides sensitivity and selectivity, we also evaluated the stability of the sensor. The operational stability and the storage stability of the glucose sensor were shown in Figure S10. The sensor gave stable chronoamperometric responses in 6 h operation and 8 days of storage.

We demonstrated the feasibility of the fiber-based glucose in the on-body test to monitor sweat glucose. The fiber-based glucose sensor was attached to a textile forearm band, which held the sweat to soak the sensing fibers (Figure S11a-b). As a proof-of-concept device, the glucose sensor was used to examine the change of glucose level in the sweat before and after a meal. As shown in Figure S11c, our wearable

DOI: 10.1021/acs.analchem.9b00152
Anal. Chem. 2019, 91, 6569−6576

chronoamperometric glucose sensor exhibited increased current level 1 h after the meal, but decreased 2 h after the meal. These amperometric responses are consistent with the glucose level in the sweat expected for a healthy human.

CONCLUSIONS

In conclusion, this work demonstrated the first proof-of-concept device of a highly stretchable gold fiber-based glucose sensor for monitoring glucose in the sweat. The effective combination of intrinsic stretchability of highly conductive gold fiber with the extrinsic helix structure led to a strain-insensitive reproducible electrochemical performance from 0 to 200% strain. Gold fibers enabled facile surface functionalization allowing textile integration of three-fiber electrodes. The glucose biosensors could function in highly stretched states and in artificial sweats, demonstrating promising applications in real-world wearable biological diagnostics anytime anywhere.

ASSOCIATED CONTENT

Supporting Information

The Supporting Information is available free of charge on the ACS Publications website at DOI: 10.1021/acs.analchem.9b00152.

Additional information about the TEM images of the ultrathin AuNWs, photographs of the dry spinning process and of the stretchable glucose sensor on an elastic sock, SEM and EDX mapping images of the electrodes, CV curves of the stretchable Au fiber and of the 80° helix fiber, stability of the glucose sensor, on-body test of the glucose sensor, and comparison of performance of the glucose sensor with reported sensors (PDF)

AUTHOR INFORMATION

Corresponding Author

*E-mail: wenlong.cheng@monash.edu.

ORCID

Qianqian Shi: 0000-0001-8787-8227

Wenlong Cheng: 0000-0002-2346-4970

Notes

The authors declare no competing financial interest.

ACKNOWLEDGMENTS

We thank the Australian Research Council via Discovery Grant scheme DP180101715 and Linkage Project LP160100521 for financial support. This work was performed in part at the Melbourne Centre for Nanofabrication (MCN) in the Victorian Node of the Australian National Fabrication Facility (ANFF). We also gratefully acknowledge the use of facilities at the Monash Centre for Electron Microscopy. T. An thanks the financial aid from Chinese Scholarship Council (CSC).

REFERENCES

(1) Pang, C.; Koo, J. H.; Nguyen, A.; Caves, J. M.; Kim, M. G.; Chortos, A.; Kim, K.; Wang, P. J.; Tok, J. B. H.; Bao, Z. *Adv. Mater.* **2015**, *27*, 634−640.

(2) Gong, S.; Schwalb, W.; Wang, Y.; Chen, Y.; Tang, Y.; Si, J.; Shirinzadeh, B.; Cheng, W. *Nat. Commun.* **2014**, *5*, 3132.

(3) Liu, Z.; Qi, D.; Guo, P.; Liu, Y.; Zhu, B.; Yang, H.; Liu, Y.; Li, B.; Zhang, C.; Yu, J.; Liedberg, B.; Chen, X. *Adv. Mater.* **2015**, *27*, 6230−6237.

(4) Rogers, J. A.; Someya, T.; Huang, Y. *Science* **2010**, *327*, 1603−1607.

(5) Imani, S.; Bandodkar, A. J.; Mohan, A. M. V.; Kumar, R.; Yu, S.; Wang, J.; Mercier, P. P. *Nat. Commun.* **2016**, *7*, 11650.

(6) Wang, Y.; Gong, S.; Wang, S. J.; Yang, X.; Ling, Y.; Yap, L. W.; Dong, D.; Simon, G. P.; Cheng, W. *ACS Nano* **2018**, *12*, 9742−9749.

(7) Nyein, H. Y. Y.; Tai, L.-C.; Ngo, Q. P.; Chao, M.; Zhang, G. B.; Gao, W.; Bariya, M.; Bullock, J.; Kim, H.; Fahad, H. M.; Javey, A. *ACS Sensors* **2018**, *3*, 944−952.

(8) Gao, W.; Emaminejad, S.; Nyein, H. Y. Y.; Challa, S.; Chen, K.; Peck, A.; Fahad, H. M.; Ota, H.; Shiraki, H.; Kiriya, D.; Lien, D.-H.; Brooks, G. A.; Davis, R. W.; Javey, A. *Nature* **2016**, *529*, 509−514.

(9) Yu, Y.; Zhai, J.; Xia, Y.; Dong, S. *Nanoscale* **2017**, *9*, 11846−11850.

(10) Bariya, M.; Nyein, H. Y. Y.; Javey, A. *Nat. Electron.* **2018**, *1*, 160−171.

(11) Vashist, S. K. *Anal. Chim. Acta* **2012**, *750*, 16−27.

(12) Moyer, J.; Wilson, D.; Finkelshtein, I.; Wong, B.; Potts, R. *Diabetes Technol. Ther.* **2012**, *14*, 398−402.

(13) Sakaguchi, K.; Hirota, Y.; Hashimoto, N.; Ogawa, W.; Hamaguchi, T.; Matsuo, T.; Miyagawa, J.-I.; Namba, M.; Sato, T.; Okada, S.; Tomita, K.; Matsuhisa, M.; Kaneto, H.; Kosugi, K.; Maegawa, H.; Nakajima, H.; Kashiwagi, A. *J. Diabetes Sci. Technol.* **2013**, *7*, 678−688.

(14) Chen, C.; Xie, Q.; Yang, D.; Xiao, H.; Fu, Y.; Tan, Y.; Yao, S. *RSC Adv.* **2013**, *3*, 4473.

(15) Kim, J.; Campbell, A. S.; Wang, J. *Talanta* **2018**, *177*, 163−170.

(16) Lee, H.; Hong, Y. J.; Baik, S.; Hyeon, T.; Kim, D.-H. *Adv. Healthcare Mater.* **2018**, *7*, 1701150.

(17) Bandodkar, A. J.; Jeerapan, I.; Wang, J. *ACS Sensors* **2016**, *1*, 464−482.

(18) Xuan, X.; Yoon, H. S.; Park, J. Y. *Biosens. Bioelectron.* **2018**, *109*, 75−82.

(19) Bandodkar, A. J.; Jia, W.; Yardımcı, C.; Wang, X.; Ramirez, J.; Wang, J. *Anal. Chem.* **2015**, *87*, 394−398.

(20) Zhang, X.; Jing, Y.; Zhai, Q.; Yu, Y.; Xing, H.; Li, J.; Wang, E. *Anal. Chem.* **2018**, *90*, 11780−11784.

(21) Lee, H.; Song, C.; Hong, Y. S.; Kim, M. S.; Cho, H. R.; Kang, T.; Shin, K.; Choi, S. H.; Hyeon, T.; Kim, D. *Sci. Adv.* **2017**, *3*, e1601314.

(22) Bandodkar, A. J.; Jeerapan, I.; You, J.-M.; Nuñez-Flores, R.; Wang, J. *Nano Lett.* **2016**, *16*, 721−727.

(23) Jeerapan, I.; Sempionatto, J. R.; Pavinatto, A.; You, J.-M.; Wang, J. *J. Mater. Chem. A* **2016**, *4*, 18342−18353.

(24) Gong, S.; Cheng, W. *Adv. Electron. Mater.* **2017**, *3*, 1600314.

(25) An, T.; Cheng, W. *J. Mater. Chem. A* **2018**, *6*, 15478−15494.

(26) Abellán-Llobregat, A.; Jeerapan, I.; Bandodkar, A.; Vidal, L.; Canals, A.; Wang, J.; Morallón, E. *Biosens. Bioelectron.* **2017**, *91*, 885−891.

(27) Lee, H.; Choi, T. K.; Lee, Y. B.; Cho, H. R.; Ghaffari, R.; Wang, L.; Choi, H. J.; Chung, T. D.; Lu, N.; Hyeon, T.; Choi, S. H.; Kim, D.-H. *Nat. Nanotechnol.* **2016**, *11*, 566−572.

(28) Weng, W.; Chen, P.; He, S.; Sun, X.; Peng, H. *Angew. Chem., Int. Ed.* **2016**, *55*, 6140−6169.

(29) Zeng, W.; Shu, L.; Li, Q.; Chen, S.; Wang, F.; Tao, X.-M. *Adv. Mater.* **2014**, *26*, 5310−5336.

(30) Sun, H.; Zhang, Y.; Zhang, J.; Sun, X.; Peng, H. *Nat. Rev. Mater.* **2017**, *2*, 17023.

(31) Heo, J. S.; Eom, J.; Kim, Y.-H.; Park, S. K. *Small* **2018**, *14*, 1703034.

(32) Wang, L.; Wang, L.; Zhang, Y.; Pan, J.; Li, S.; Sun, X.; Zhang, B.; Peng, H. *Adv. Funct. Mater.* **2018**, *28*, 1804456.

(33) Zhu, B.; Gong, S.; Cheng, W. *Chem. Soc. Rev.* **2019**, *48*, 1668−1711.

(34) Gong, S.; Zhao, Y.; Shi, Q.; Wang, Y.; Yap, L. W.; Cheng, W. *Electroanalysis* **2016**, *28*, 1298−1304.

(35) Zhu, W.; Zhang, Y.; Zhou, X.; Xu, J.; Liu, Z.; Yuan, N.; Ding, J. *Nanoscale Res. Lett.* **2017**, *12*, 448.

DOI: 10.1021/acs.analchem.9b00152
Anal. Chem. 2019, 91, 6569−6576

(36) Wang, Y.; Gong, S.; Dong, D.; Zhao, Y.; Yap, L. W.; Shi, Q.; An, T.; Ling, Y.; Simon, G. P.; Cheng, W. *Nanoscale* **2018**, *10*, 15948−15955.
(37) Zhai, Q.; Wang, Y.; Gong, S.; Ling, Y.; Yap, L. W.; Liu, Y.; Wang, J.; Simon, G. P.; Cheng, W. *Anal. Chem.* **2018**, *90*, 13498−13505.
(38) Liu, Y.-L.; Jin, Z.-H.; Liu, Y.-H.; Hu, X.-B.; Qin, Y.; Xu, J.-Q.; Fan, C.-F.; Huang, W.-H. *Angew. Chem., Int. Ed.* **2016**, *55*, 4537−4541.
(39) Liu, Y.-L.; Qin, Y.; Jin, Z.-H.; Hu, X.-B.; Chen, M.-M.; Liu, R.; Amatore, C.; Huang, W.-H. *Angew. Chem., Int. Ed.* **2017**, *56*, 9454−9458.
(40) Wang, Y.-W.; Liu, Y.-L.; Xu, J.-Q.; Qin, Y.; Huang, W.-H. *Anal. Chem.* **2018**, *90*, 5977−5981.
(41) Zhao, Y.; Dong, D.; Gong, S.; Brassart, L.; Wang, Y.; An, T.; Cheng, W. *Adv. Electron. Mater.* **2019**, *5*, 1800462.
(42) Zhao, Y.; Dong, D.; Wang, Y.; Gong, S.; An, T.; Yap, L. W.; Cheng, W. *ACS Appl. Mater. Interfaces* **2018**, *10*, 42612−42620.
(43) Feng, H.; Yang, Y.; You, Y.; Li, G.; Guo, J.; Yu, T.; Shen, Z.; Wu, T.; Xing, B. *Chem. Commun.* **2009**, 1984−1986.
(44) Chen, Y.; Ouyang, Z.; Gu, M.; Cheng, W. *Adv. Mater.* **2013**, *25*, 80−85.
(45) Reiser, B.; Gerstner, D.; Gonzalez-Garcia, L.; Maurer, J. H. M.; Kanelidis, I.; Kraus, T. *Phys. Chem. Chem. Phys.* **2016**, *18*, 27165−27169.
(46) Reiser, B.; Gerstner, D.; Gonzalez-Garcia, L.; Maurer, J. H. M.; Kanelidis, I.; Kraus, T. *ACS Nano* **2017**, *11*, 4934−4942.
(47) Ansar, S. M.; Ameer, F. S.; Hu, W.; Zou, S.; Pittman, C. U.; Zhang, D. *Nano Lett.* **2013**, *13*, 1226−1229.
(48) Trasatti, S.; Petrii, O. A. *Pure Appl. Chem.* **1991**, *63*, 711−734.
(49) Wang, C. H.; Yang, C.; Song, Y. Y.; Gao, W.; Xia, X. H. *Adv. Funct. Mater.* **2005**, *15*, 1267−1275.
(50) Lu, Z.; Foroughi, J.; Wang, C.; Long, H.; Wallace, G. G. *Adv. Energy Mater.* **2018**, *8*, 1702047.
(51) Oh, S. Y.; Hong, S. Y.; Jeong, Y. R.; Yun, J.; Park, H.; Jin, S. W.; Lee, G.; Oh, J. H.; Lee, H.; Lee, S.-S.; Ha, J. S. *ACS Appl. Mater. Interfaces* **2018**, *10*, 13729−13740.
(52) Jiang, D.; Liu, Z.; Wu, K.; Mou, L.; Ovalle-Robles, R.; Inoue, K.; Zhang, Y.; Yuan, N.; Ding, J.; Qiu, J.; Huang, Y.; Liu, Z. *Polymers* **2018**, *10*, 375.

DOI: 10.1021/acs.analchem.9b00152
Anal. Chem. 2019, 91, 6569−6576